

A Radio Quasi-periodic Oscillation of 176 day in the Radio-loud Narrow-line Seyfert 1 Galaxy J0849+5108

PENGFEEI ZHANG¹ AND ZHONGXIANG WANG^{1,2}

¹*Department of Astronomy, School of Physics and Astronomy, Key Laboratory of Astroparticle Physics of Yunnan Province, Yunnan University, Kunming 650091, People's Republic of China; zhangpengfei@ynu.edu.cn; wangzx20@ynu.edu.cn*

²*Shanghai Astronomical Observatory, Chinese Academy of Sciences, 80 Nandan Road, Shanghai 200030, People's Republic of China*

ABSTRACT

We analyze the 11-year long-term light curve of the Radio-loud Narrow-line Seyfert 1 (NLSy1) galaxy J0849+5108 and the nearly simultaneous γ -ray data of the source. The data were obtained with the Owens Valley Radio Observatory 40-m telescope at 15 GHz and with the Large Area Telescope onboard *Fermi Gamma-ray Space Telescope*, respectively. A quasi-periodic oscillation (QPO) signal at a significance of $>5\sigma$ is found in the radio light curve, but no similar modulation is seen in the γ -ray light curve. The QPO signal was present for 21 cycles, the longest among the reported radio QPOs, and likely disappeared after 2019 January 16. Different mechanisms proposed to explain the observed QPOs in Active Galactic Nuclei (AGN) are discussed for this QPO case. Either a secular instability in the inner accretion disk or a helical structure in the jet of J0849+5108 may explain the radio QPO, while for the latter scenario the jet has to be collimated up to ~ 200 pc, similar to that seen in the nearby AGN M87. It will be of interests to keep monitoring the source at radio frequencies, seeing if similar QPO signals would appear again or not.

Keywords: galaxies: active - galaxies: individual: J0849+5108 - quasi-periodic oscillation

1. INTRODUCTION

Active Galactic Nuclei (AGN) are objects of great interest, as they contain an active supermassive black hole (SMBH) at their center and $\sim 10\%$ of them have relativistic jets. Emission from them ranging from MHz radio frequencies to TeV γ -ray energies can be mostly dominated by non-thermal radiation and variable on a variety of timescales and amplitudes. Among phenomena related to their variability, there is very intriguing one, the so-called quasi-periodic oscillations (QPOs), which have more and more cases reported recently. The QPOs were found at all frequencies from radio to GeV (or even TeV) γ -rays and their periods span over a wide range of timescales from minutes to years.

After the launch of the *Fermi Gamma-ray Space Telescope (Fermi)*, a few cases of periodic signals in γ -rays from AGN were reported. Possible QPOs of PG 1553+113, PKS 2155–304, PKS 0301–243, PKS 0537–441, PKS 0426–380, PKS 0601–70, and PMN J0948+0022 have been studied by Ackermann et al. (2015), Sandrinelli et al. (2014, 2016a,b), Zhang et al. (2017a,b,c, 2020), and Zhang et al. (2017). Their periods span in the range of ~ 1 –3 years. Interestingly, in a blazar-type AGN PKS 2247–131, a 34.5-day QPO after an initial flux peak of an outburst was reported by

Zhou et al. (2018), and it has been the only one having relatively short, monthly period in γ -rays thus far.

In X-rays, a significant QPO was reported in RE J1034+396 by Gierliński et al. (2008). Then other possible QPOs were detected in Mrk 766, 2XMM J123103.2+110648, and 1H 0707–495 (Zhang et al. 2017d; Lin et al. 2013; Pan et al. 2016; Zhang et al. 2018). The peculiar case is in 1H 0707–495, in which double QPOs appeared and were separated by an intermediate state with a frequency ratio of $\sim 1:2$ (Zhang et al. 2018). Different from those found in γ -rays, these QPOs have very short periods, ~ 1 –3 hrs. They possibly follow the correlation between QPO frequency and black-hole mass M_{BH} , as suggested in Kluzniak & Abramowicz (2002); Remillard & McClintock (2006); Zhou et al. (2010); Zhou et al. (2015); Pan et al. (2016); Zhang et al. (2017d, 2018).

In optical band, the most well-known case is OJ 287, which exhibits ~ 12 -yr periodicity in its optical light curve based on more than a century monitoring (Kidger et al. 1992; Fan & Lin 2000; Valtonen et al. 2006, 2008). In PKS 2155–304, a 317 day QPO was found in the optical light curve on a ~ 3600 -day long-term time scale (Zhang et al. 2014). Interestingly this period

is exactly half of that of the QPO detected in γ -rays (Sandrinelli et al. 2014; Zhang et al. 2017a).

Several cases of AGN QPOs were also found in radio light curves. In CGRABS J1359+4011, a QPO exhibiting 150 day period was reported by King et al. (2013). Bhatta (2017) claimed a QPO having 270-day period in PKS 0219–164. 1ES 1959+650, J1043+2408, and PKS J0805–0111 were also reported to have possible QPO behavior (Li et al. 2017; Bhatta 2018; Ren et al. 2020). These radio QPOs have periods ranging from approximately half a year up to several years, similar to those of QPOs found in γ -rays.

While the drastically different timescales of the periodic signals found in such as X-rays and γ -rays are likely due to the selection effect caused by the observational modes—no sensitive X-ray telescopes would spend valuable time to monitor AGN for years (also see Vaughan & Uttley 2005 for detectability of X-ray QPOs in AGN) and *Fermi* does not have sufficiently high sensitivity to monitor many AGN on minute-long timescales, they have been discussed to indicate different physical processes. For example, the sub-day QPOs have been compared to those found in stellar-mass black hole systems and are thought to similarly reflect accretion activities near a SMBH (e.g., Gierliński et al. 2008), while the year-long ones are generally considered to be the indicator of binary SMBH systems (e.g., Ackermann et al. 2015). Because of the middle position in the periodicity range of QPOs, the month-long one in PKS 2247–131 was interpreted to be due to the helical structure in the jet (Zhou et al. 2018). Therefore QPOs could serve as a unique probe to help reveal structures and physical processes of AGN.

In this paper we report a discovery of a QPO at ~ 176 day with a significance of over 5σ in radio emission from a Radio-loud Narrow-line Seyfert 1 (NLSy1) galaxy, J084957.97+510829.0 (hereafter J0849+5108). The radio light curve was obtained from monitoring observations of J0849+5108 with the Owens Valley Radio Observatory (OVRO) 40-m telescope. As *Fermi* provided monitoring of the source nearly simultaneous, we also analyzed the γ -ray data. Below we first summarize the properties of J0849+5108 in section 1.1. In section 2, we describe the analysis for the OVRO radio light curve and *Fermi* γ -ray data and show the main results. In section 3 the results are discussed.

1.1. NLSy1 galaxy J0849+5108

The NLSy1 galaxies are a subclass of AGN (Osterbrock & Pogge 1985; Mathur 2000), containing black holes at the low end of the AGN M_{BH} range ($10^5 - 10^8 M_{\odot}$; Zhou et al. 2006; Xu et al. 2012) and

having high Eddington accretion rates (between 0.1–1; Boller et al. 1996). A few percent of them are radio loud, indicating the presence of relativistic jets (Komossa et al. 2006; Lister 2018), and some show jet morphologies on parsec scales (Doi et al. 2007; Gu & Chen 2010). J0849+5108 is one of the most studied NLSy1 galaxies (see D’Ammando et al. 2012; Maune et al. 2014 and references therein). The central black hole was estimated to have $M_{\text{BH}} \sim 10^{7.4} M_{\odot}$ (Yuan et al. 2008). Since 2011 June, γ -ray flares from it were detected with *Fermi*. Combined with radio studies, the high-energy detection confirmed the presence of a jet in it (D’Ammando et al. 2012). High-resolution radio observations resolved its radio emission, and a jet structure was seen extending from the radio core to several tens of parsec projected distance (D’Ammando et al. 2012; Lister et al. 2018). Based on broadband studies and its strong brightness variability, its similarity with the blazar-like AGN (Maune et al. 2014) has been established, i.e., the jet is pointing close to our line of sight (Paliya et al. 2016).

In this paper, the cosmological parameters from the Planck mission (Planck Collaboration et al. 2014) are used (the Hubble constant $H_0 \simeq 67 \text{ km s}^{-1} \text{ Mpc}^{-1}$). The redshift of the source $z \simeq 0.584$ (Alam et al. 2015) corresponds to the luminosity distance of $\sim 3500 \text{ Mpc}$.

2. DATA ANALYSIS AND RESULTS

2.1. OVRO light curve data

The OVRO 40-m telescope has been monitoring over 1800 AGN¹ twice a week at 15 GHz since 2008. The obtained data are reduced and calibrated to form light curves available on their publicly accessible database². The flux density scale is derived using the primary calibrator 3C 286, and the detailed information about the observing program, data reduction, and calibration procedure are described in Readhead et al. (1989); Richards et al. (2011). The source J0849+5108 (R.A. = $08^{\text{h}}49^{\text{m}}58^{\text{s}}.080$, decl. = $51^{\circ}08'29''.040$) is one of the OVRO’s targets. It has been observed for approximately 11 years (from 2009 March 28 to 2020 June 22). We show its radio light curve in the bottom panel of Figure 1. The minimum and median time intervals of two adjacent time bins are ~ 0.68 and 5.6 days respectively, and the maximum interval is ~ 92 days at MJD 56823.6 (marked with a green cross in Figure 1). In the light curve, the minimum (at MJD 56380.32), maximum (at MJD 56980.71), and mean value (shown with a red hor-

¹ <https://sites.astro.caltech.edu/ovroblazars/index.php?page=sourcelist>

² <https://sites.astro.caltech.edu/ovroblazars>

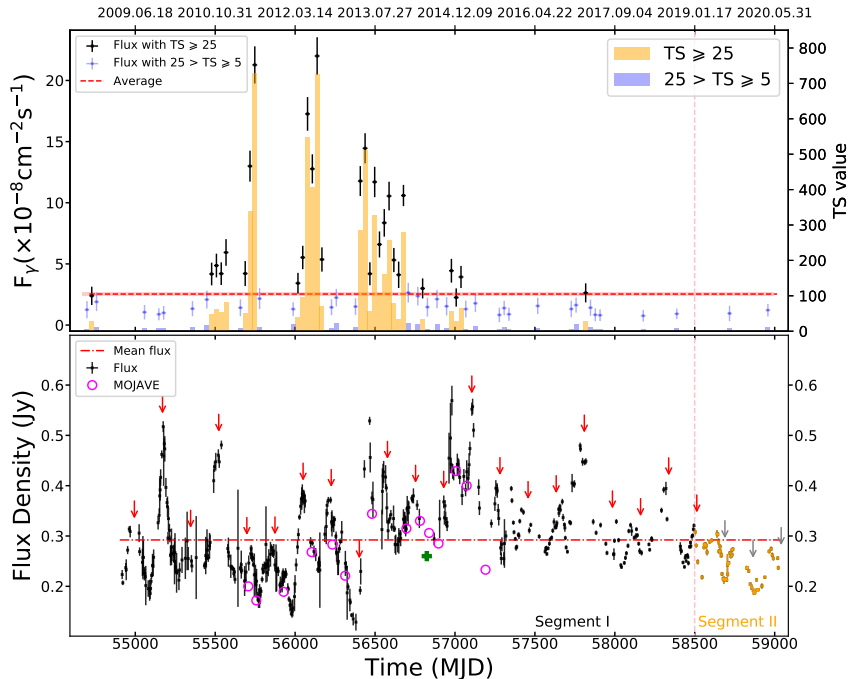


Figure 1. Light curves of the NLSy1 galaxy J0849+5108. *Bottom* panel: 15-GHz flux density curve obtained with the OVRO 40-m telescope. The green cross marks the maximum interval between two data points and the red horizontal dotted-dashed line is the mean flux density of the radio light curve. The pink vertical dashed line marks the position after which the QPO vanishes (data points in orange color), and the arrows indicate the expected flux maxima for every cycles. The peak intensity measurements of the source’s radio emission at 15 GHz from the MOJAVE survey (Lister et al. 2018) are indicated by purple circles. *Top* panel: 0.1–500 GeV γ -ray monthly light curve, for which the TS values of the data points are given by orange ($TS \geq 25$) and light blue ($25 > TS \geq 5$) bars. The data points in these two TS ranges are marked with black and light blue color correspondingly. The red dashed line represents the average integrated photon flux over the whole time period.

izontal dotted-dashed line) are 0.12, 0.57, and 0.29 Jy respectively, and its standard deviation is 7.7%.

2.2. Fermi Large Area Telescope data

The source J0849+5108 was detected with the Large Area Telescope (LAT) onboard *Fermi* (Atwood et al. 2009). It is named as 4FGL J0850.0+5108 in the fourth Fermi Large Area Telescope catalog (4FGL; Abdollahi et al. 2020). We selected *Fermi*-LAT 0.1–500 GeV Pass 8 (*Front+Back* SOURCE class) photon-like events from the LAT data between 2008 August 4 and 2020 August 28 within a $20^\circ \times 20^\circ$ region centered at the position of J0849+5108. The events were reduced by requiring the zenith angle $< 90^\circ$, $DATA_QUAL > 0$, and $LAT_CONFIG = 1$. A binned maximum likelihood analysis was performed to the selected events data using the instrument response files (P8R3_SOURCE_V2) and the 4FGL model (Abdollahi et al. 2020). In 4FGL, emission of J0849+5108 is described with a log-parabolic spectrum model. From the analysis, the integrated photon flux in the 0.1–500 GeV energy range was obtained to be $(22.8 \pm 1.3) \times 10^{-9}$ photons $\text{cm}^{-2} \text{s}^{-1}$ with a test statistic (TS) value of ~ 2940 . The best-fit photon spectral parameters α ,

β , and E_b were 2.18 ± 0.04 , 0.07 ± 0.02 , and 649 ± 90 MeV, respectively. These values are in agreement with those reported in 4FGL (Abdollahi et al. 2020). The best-fitting results were saved as a new model file. We then obtained light curves of the source based on this new model file.

The source’s γ -ray emission was generally due to three major flares, although the third one (at MJD 56500) shows complex variation structures. Different time bins were tested when we constructed a light curve, and we found that a monthly (30-day bin) light curve depicts the overall variation features of the source (see Figure 1). For this light curve, we considered a data point with $TS \geq 25$ ($\gtrsim 5\sigma$) as a detection, while those data points with $25 > TS \geq 5$ were also included in order to show the flux variations as complete as possible. The TS values of the data points are given in Figure 1, where the two TS ranges are marked with orange and light blue color respectively.

2.3. Temporal variability analysis and results

To search for periodicity in the OVRO radio light curve of J0849+5108 by calculating a power spectrum, we first employed the method of the Weighted Wavelet

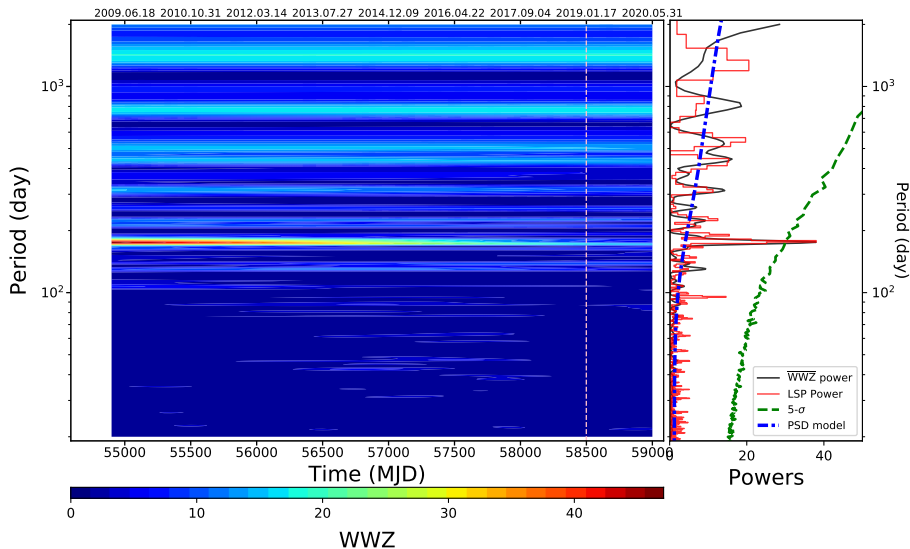


Figure 2. Power spectra of the J0849+5108 OVRO light curve. *Left* panel: the color-scaled WWZ power spectrum calculated in a range of frequencies over the time duration of the whole light curve. *Right* panel: time-averaged WWZ power spectrum (black curve) and LSP power spectrum (red histogram), calculated from the data before MJD 58500 (marked by the dashed vertical line in the left panel). The blue dashed-dotted line is the best-fit underlying PSD, and the green dashed line is the 5σ confidence curve evaluated from artificial light curves.

Z-transform (WWZ; Foster 1996). In WWZ, the wavelet transform is casted as a weighted projection and observed fluxes are compared to Morlet wavelet functions instead of sinusoids (Foster 1996), and the method captures frequency and location information (here in time) simultaneously by changing the parameters of wavelets. For non-persistent periodic signals, WWZ can show when a periodic signal starts to decrease. We obtained color-scaled WWZ power spectrum for the whole light curve, which is shown in the left panel of Fig. 2. A signal is seen at ~ 176 days. The time-averaged WWZ power spectrum (averaged at frequencies along time) was also obtained, and careful examination of the power value of it allowed us to find that the power value increases to the maximum at MJD 58499.22 (2019 January 16, marked with pink vertical dashed line in Figure 1) but then starts decreasing. We thus divided the light curve into two segments (see the bottom panel of Figure 1): Segment I (black) and Segment II (orange). The time-averaged WWZ power spectrum in Segment I is shown in the right panel of Figure 2. A QPO signal has a peak at 175.93 ± 6.34 days, where the uncertainty was estimated as the full width at half maximum of a Gaussian function that fits the power peak.

We then used the generalized Lomb-Scargle Periodogram (LSP; Lomb 1976; Scarle 1982; Zechmeister & Kürster 2009) as an independent check for the result from the WWZ method. The LSP method is a common tool in time series analysis for unequally spaced data, and can provide accurate frequencies and power spec-

tral intensities (Zechmeister & Kürster 2009). Only the light curve in Segment I was analyzed. The resulting power spectrum is shown as the red histogram in Figure 2. A sharp peak around 176 days, nearly the same as that from the WWZ method, was revealed. The results confirm the signal detection from the WWZ method.

We used the period to calculate the expected flux maxima for every cycles, which are shown as red arrows in the bottom panel of Figure 1. It can be seen that although the light curve overall has large variations, the arrows in most cases point at the local flux maxima in the light curve. It can also be noted that in Segment II the arrows start missing the flux maxima, supporting the result from our above WWZ analysis that the signal starts decreasing after \sim MJD 58500.

For the power peak, the probability p to obtain a power equal to or higher than the threshold from a chance fluctuation is $< 5.9 \times 10^{-19}$, and the false-alarm probability (FAP = $1 - (1 - p)^N$) is 1.2×10^{-16} (Horne & Baliunas 1986; Zechmeister & Kürster 2009), where N is the number of independent frequencies sampled (i.e., the trial factor). To estimate the underlying power spectral density (PSD), we used a function of smoothly bending power-law plus a constant (González-Martín & Vaughan 2012) to model the PSD calculated from the light curve. A maximum likelihood method was employed (Barret & Vaughan 2012). The PSD function has a form of $P(f) = Af^{-\alpha}[1 + (f/f_{bend})^{\beta-\alpha}]^{-1} + C$, where A , α , β , f_{bend} , and C are the normalization, low frequency slope, high frequency slope, bend frequency,

and Poisson noise, respectively, and the obtained values are 1.12 ± 0.84 , 0.33 ± 0.03 , 2.73 ± 0.69 , 0.0059 ± 0.0016 , and 1.19 ± 0.06 , respectively. To evaluate a confidence level for the periodic signal, we generated 10^7 artificial light curves based on the best-fit underlying PSD and probability density function of the flux density variations by employing the simulation program provided in Emmanoulopoulos et al. (2013). The confidence curve evaluated from the artificial light curves is shown as a green line in the right panel of Figure 2. The confidence level for the QPO signal was found to be $> 5\sigma$.

We also checked the γ -ray light curve for any similar QPO signals. However the light curve mainly consists of three major flares and no QPO signals were found. We note that the third flare shows repeated sub-flare structures, which is discussed below.

3. DISCUSSION

We have analyzed the OVRO 15-GHz light curve of J0849+5108 from 2009 March to 2020 June, and found a QPO with a period of 176 day at a significance of $> 5\sigma$ in the data before 2019 January. Compared to the previous QPO cases reported in radio light curves of AGN, this QPO lasted the most cycles (21 cycles) and had a significance similar to or even higher than most of the others. The QPO signal likely disappeared after 2019 January; for example, if the whole light curve is considered, the significance of the signal would become much lower. This transient nature makes it fit the other reported QPOs, as most of them are transient phenomena. It is of interest to keep monitoring the source, checking how its radio emission varies and whether or not the QPO signal would appear again.

The nearly simultaneous *Fermi*-LAT data were also analyzed, but only three major flaring events were detected and no similar periodic pattern was seen. D’Ammando et al. (2013) suggested that the γ -ray flare around MJD 56100 was connected to the radio brightening around MJD 56200–56300 (i.e., related but delayed radio activity), but our result indicates that the radio brightening actually was only one of the QPO cycles, not likely related to the γ -ray flaring events. However the delayed radio activity maybe was seen in the third major flare in year 2013. Maune et al. (2014) presented broadband monitoring data covering the early half of year 2013, which contain the OVRO light curve during the time period. In Figure 3, we show the details of the γ -ray and radio light curves in 2013–2014, where we used 15 day for the time bin of the former. The 2013 flare appears to consist of four subflares (indicated by fluxes and > 200 TS values), the first of which was discussed in Maune et al. (2014). They reported optical

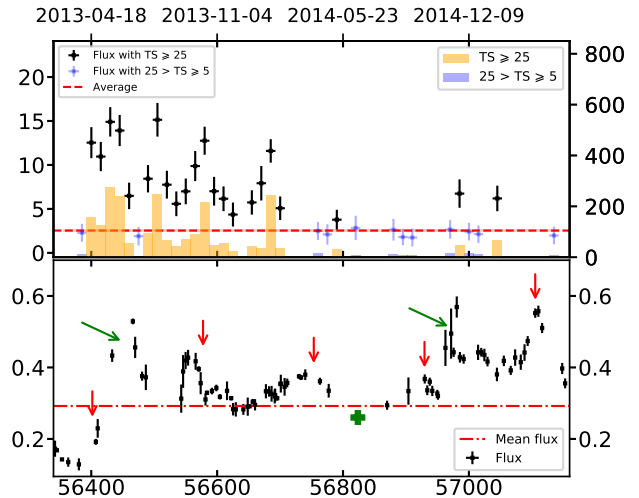


Figure 3. Same as Figure 1, but the time bin of the γ -ray light curve is 15 days. Two radio flux density peaks, in addition to the peaks of the QPO cycles, are marked by green arrows.

and X-ray flux as well as optical polarization measurements, which show significant variations related to the γ -ray flare (or the first subflare), and suggested a radio peak (marked by the first green arrow in Figure 3) as the delayed activity. This radio peak indeed is not one of the QPO cycles, and also we note that the following peak mismatches (and occurs before) the red arrow by ~ 25 days (four times that the uncertainty of the QPO period). In addition, the radio peak before MJD 57000 (marked by the second green arrow) is similarly not one of the QPO cycles, and it coincides with a minor γ -ray flaring event—a $TS > 200$ γ -ray data point around the same time. Therefore it is reasonable to consider that these radio variations were possibly related to the γ -ray flaring activities. While it has been established from simultaneous monitoring at radio and γ -rays that few of blazars show correlated variations at the two bands (Max-Moerbeck et al. 2014), we suggest that the radio emission of J0849+5108 may contain two components: one the baseline that shows the QPO and the other related to additional activities of the system including the γ -ray flares.

Possible mechanisms behind the QPOs in AGN have been widely discussed (see, e.g., King et al. 2013; Ackermann et al. 2015 and references therein). Since QPOs in stellar-mass black-hole binary systems have been well studied, and in most cases they were interpreted to be related to the accretion in the innermost stable circular orbit around black holes (Remillard & McClintock 2006), the similar scenario was considered for AGN QPOs. The most notable case is the X-ray QPO found in RE J1034+396 (Gierliński et al. 2008), which had

1-hr period. Scaling different frequencies of QPOs in stellar-mass black holes to the 1-hr periodicity, a mass range of $4 \times 10^5 - 10^7 M_\odot$ was found for the SMBH in RE J1034+396. We note that this source is also a NLSy1 galaxy, the same as J0849+5108. If we apply the same scenario to the target, an extremely massive black hole ($> 10^9 M_\odot$) would be implied, in contradiction to the general M_{BH} range of NLSy1 and the estimated mass of the SMBH in J0849+5108. A related scenario is that the jet is precessing, caused by the Lense-Thirring precession of the accretion disk around the black hole. This scenario has been widely considered for QPOs seen in stellar-mass black hole systems (see Ingram & Motta 2020 and references therein). However the above mass-mismatch problem remains as the timescales of the periodicities are expected to scale with M_{BH} .

Generally in the coupled disk-jet systems, periodic changes in an accretion disk would be reflected by jet activities. There are several scenarios that could lead to the QPO phenomena. Simulations show that magnetically choked accretion flows (or magnetically arrested disks) could produce quasi-periodic signals (Tchekhovskoy et al. 2011; McKinney et al. 2012). However the timescales of the predicted signals are generally short, ~ 1 day, not matching that of J0849+5108. For thick disks around black holes, it has been shown that under an external perturbation, acoustic p-mode oscillations can be excited. The excited frequencies are related to the radial epicyclic frequency (Rubio-Herrera & Lee 2015a,b). For the 176-day period and $M_{\text{BH}} \sim 10^{7.4} M_\odot$, the typical radius can be estimated to be $\sim 360 r_g$, where r_g is the gravitational radius. The scenario of such a disk in J0849+5108 is possible. However, multiple frequencies following the ratio of 2:3... are predicted in numerical simulations (Rubio-Herrera & Lee 2015a,b), which were likely seen in the periodic radio variability cases of the blazars NRAO 530 and 1156+295 (An et al. 2013; Wang et al. 2014). In J0849+5108, we did not see multiple frequencies. The 176-day period is similar to that of the QPO in the blazar J1359+4011, determined to be $\sim 120-150$ days (King et al. 2013). The Lightman-Eardley secular instability (Lightman & Eardley 2013), applicable to the black hole systems with high Eddington accretion rates, was suggested to explain the QPO case of J1359+4011. By the same token and given the high Eddington ratio property of the NLSy1, the instability scenario should be applicable to J0849+5108 as well.

For year-long QPOs, their indication for the existence of a binary SMBH system at the center of AGN has been intriguingly discussed (e.g., Valtonen et al. 2008; Ackermann et al. 2015). The secondary SMBH may

induce an observable periodic signal, which reflects the orbital periodicity of the binary. However the period of 176 day is rather too short. The intrinsic period at the local galaxy would be $176/(1+z) \simeq 111$ days. The period suggests a very tight orbit (a binary separation of ~ 0.001 pc) and a quick merging time scale (~ 760 years) due to gravitational radiation, where the mass ratio between the two SMBHs is assumed to be 1 (see details in Sobacchi et al. 2017).

Finally, since the radio emission of J0849+5108 arises from its jet, the jet activity and structure could directly lead to the QPO signal. The source is a target in the MOJAVE survey and multiple Very Long Baseline Array (VLBA) imaging of it during 2011–2016 are available (Lister et al. 2018). We mark the peak intensities from the observations in Figure 1 (purple circles). As can be seen, their variations are generally consistent with those of the OVRO light curve. We checked the individual VLBA images. Although no images were taken at any peak of the QPO variations, a jet structure is seen to be nearly always present in the images extending from the core to 3–4 milli-arcseconds. No evidence is seen showing the QPO variations as the results of new, emerging radio components. Recently a helical structure of jets has been invoked to explain the 34.5 day QPO observed in PKS 2247–131 (Zhou et al. 2018). As an emitting blob in a jet moves along a helical path, our viewing angle to it changes giving rise to quasi-periodic flux modulation due to the Doppler beaming effect. Helicity is likely a natural feature in magnetically dominated jets (Chen & Zhang 2020). For the case of J0849+5108, if we assume the parameters used in Paliya et al. (2016) for modeling the spectral energy distribution, the bulk Lorentz factor $\Gamma = 13$, the pitch angle (between the emitting blob’s motion and the jet’s axis; assumed to be half of the opening angle) $\phi = 0.1$ rad, the viewing angle $\psi = 3^\circ$, the jet observed at the radio 15 GHz frequency would have moved ~ 200 pc at the local galaxy in 21 cycles (the local cycle period would be ~ 33 yrs; Camenzind & Krockenberger 1992; Zhou et al. 2018). The distance of ~ 200 pc is not unreasonably long, as the jet in the nearby AGN M87 has been seen collimated up to a distance of ~ 300 pc (e.g., Asada et al. 2014). Also we note that high-frequency (22 and 37 GHz) imaging resolved the radio core of J0849+5108, indicating a size of 320×215 pc (Berton et al. 2018). Therefore we may explain the radio QPO of J0849+5108 as the result of the helical motion of an emitting blob. Aside from the QPO modulation, the radio light curve also shows relatively large variations, which should be caused by the emission from the whole jet. In addition, since the γ -ray emission likely arises from a site close to the central SMBH,

it thus does not share any similar variations with that at the radio frequency (Max-Moerbeck et al. 2014).

In any case, our finding of a 176 day QPO at radio in J0849+5108 presents another interesting case among AGN QPO phenomena. As more powerful facilities are available or being built, more QPO cases of different time scales at different frequencies will be found. QPOs of different time scales (e.g., intra-day, monthly, and yearly) likely do not have the same origin, and they may not appear in the same time at different observation frequencies. The case in J0849+5108 proves the latter. Multi-frequency studies of them probably will be the key for understanding their origins, by not only helping detect a case with high confidence, since most of them appear to be transient, but also providing more information to establish their properties and identify the underlying physical process among different possibilities.

ACKNOWLEDGEMENTS

We thank anonymous referee for very helpful suggestions. We also thank F. Xie for discussion about different black hole accretion scenarios and M. Gu for radio jet properties. This research has made use of data from the OVRO 40-m monitoring program which was supported in part by NASA grants NNX08AW31G, NNX11A043G and NNX14AQ89G, and NSF grants AST-0808050 and AST-1109911, and private funding from Caltech and the MPIfR. This research is supported by the National Key R&D Program of China under grant No. 2018YFA0404204, and the joint foundation of Department of Science and Technology of Yunnan Province and Yunnan University [2018FY001 (-003)]. Z. W. acknowledges the support by the National Program on Key Research and Development Project (Grant No. 2016YFA0400804), the National Natural Science Foundation of China (11633007), the Original Innovation Program of the Chinese Academy of Sciences (E085021002).

REFERENCES

- Abdollahi, S., Acero, F., Ackermann, M., et al. 2020, *ApJS*, 247, 33
- Ackermann, M., Ajello, M., Albert, A., et al. 2015, *ApJL*, 813, L41
- An, T., Baan, W. A., Wang, J., Wang, Y., Hong, X. 2013, *MNRAS*, 434, 3487
- Asada, K., Nakamura, M., Doi, A., et al. 2014, *ApJL*, 781, L2
- Atwood, W. B., Abdo, A. A., Ackermann, M., et al. 2009, *ApJ*, 697, 1071
- Alam, S., Albareti, F. D., Allende Prieto, C., et al. 2015, *ApJS*, 219, 12
- Barret, D., & Vaughan, S. 2012, *ApJ*, 746, 131
- Berton, M., Congiu, E., Järvelä, E., et al. 2018, *A&A*, 614, A87
- Bhatta, G. 2017, *ApJ*, 847, 7
- Bhatta, G. 2018, *Galax*, 6, 136
- Boller, T., Brandt, W. N., & Fink, H. 1996, *A&A*, 305, 53
- Camenzind, M. & Krockenberger, M. 1992, *A&A*, 255, 59
- Chen, L. & Zhang, B., arXiv:2010.14470
- D’Ammando, F., Orienti, M., Finke, J., et al. 2012, *MNRAS*, 426, 317
- D’Ammando, F., Orienti, M., Finke, J., et al. 2013, *MNRAS*, 436, 191
- Doi, A., Fujisawa, K., Inoue, M., et al. 2007, *PASJ*, 59, 703
- Emmanoulopoulos, D., et al. 2013, *MNRAS*, 433, 907-927
- Fan, J. H., & Lin, R. G. 2000, *A&A*, 355, 880
- Foster G. 1996, *AJ*, 112, 1709
- Gierliński, M., Middleton, M., Ward, M., & Done, C., 2008, *Nature*, 455, 369
- González-Martín, O., Vaughan, S., 2012, *A&A*, 544, A80
- Gu, M. & Chen, Y. 2010, *AJ*, 139, 2612
- Horne, J. H. & Baliunas, S. L., 1986, *ApJ*, 302, 757H
- Ingram, A. & Motta S. 2020, *New Astronomy reviews*, arXiv: 2001.08758
- Kidger, M., Takalo, L., & Sillanpaa, A. 1992, *A&A*, 264, 32
- King, O. J., Hovatta, T., Max-Moerbeck, W., et al. 2013, *MNRASL*, 436, L114-L117
- Kluzniak, W., & Abramowicz, M. A. 2002, arXiv:astro-ph/0203314
- Komossa, S., Voges, W., Xu, D., et al. 2006, *AJ*, 132, 531
- Li, X. P., Luo, Y. H., Yang, H. Y., et al., 2017, *ApJ*, 847, 8
- Lightman, A. P., & Eardley, D. M., 1974, *ApJ*, 187, L1
- Lin, D., Irwin, J. A., Godet, O., et al., 2013, *ApJL*, 776, L10
- Lister, M. 2018, in “Revisiting Narrow-Line Seyfert 1 Galaxies and their Place in the Universe”, arXiv: 1805.05258
- Lister, M. L., Aller, M. F., Aller, H. D., et al. 2018, *ApJS*, 234, 12
- Lomb, N. R. 1976, *Ap&SS*, 39, 447
- Mathur, s. 2000, *MNRAS*, 314, L17
- Max-Moerbeck, W., et al. 2014, *MNRAS*, 445, 428
- Maune, J. D., Eggen, J. R., Miller, H. R., et al. 2014, *ApJ*, 794, 93
- McKinney, J. C., Tchekhovskoy, A., & Blandford, R. D. 2012, *MNRAS*, 423, 3083

- Osterbrock, D. E., & Pogge, R. W. 1985, *ApJ*, 297, 166
- Pan, H.-W., Yuan, W.-M., Yao, S., et al., 2016, *ApJL*, 819, L19
- Paliya, V.-S., Rajput, B., Stalin, C. S., Pandey, S. B., 2016, *ApJ*, 819, 121
- Planck Collaboration, et al. 2014, *A&A*, 571, A16
- Readhead A. C. S., Lawrence C. R., Myers S. T., et al., 1989, *ApJ*, 346, 566
- Remillard, R. A., & McClintock, J. E. 2006, *ARA&A*, 44, 49
- Ren, G. W., Zhang, H. J., Zhang, X., et al. 2020, *arXiv:2009.14604*
- Richards, J. L., Max-Moerbeck, W., Pavlidou, V., et al., 2011, *ApJS*, 194, 29
- Rubio-Herrera, E., & Lee, W. H., 2005a, *MNRAS*, 357, 31
- Rubio-Herrera, E., & Lee, W. H., 2005b, *MNRAS*, 362, 789
- Sandrinelli, A., Covino, S., & Treves, A., 2014, *ApJL*, 793, L1
- Sandrinelli, A., Covino, S., Treves, A., 2016a, *ApJ*, 820, 20S
- Sandrinelli, A., Covino, S., Dotti, M., Treves, A., 2016b, *AJ*, 151, 54
- Scarle, J. D. 1982, *ApJ*, 263, 835
- Sobacchi, E., Sormani, M., & Stameria, A. 2017, *MNRAS*, 465, 161S
- Tchekhovskoy, A., Narayan, R., & McKinney, J. C. 2011, *MNRAS*, 418, L79
- Valtonen, M. J., Lehto, H. J., Sillanpü, A., et al. 2006, *ApJ*, 646, 36
- Valtonen, M. J., Lehto, H. J., Nilsson, K., et al. 2008, *Nature*, 452, 851
- Vaughan, S. & Uttley, P. 2005, *MNRAS*, 362, 235
- Wang, J., An, T., Baan, W. A., Lu, X. 2014, *MNRAS*, 443, 58
- Xu, D., et al. 2012, *AJ*, 143, 83
- Yuan, W., Zhou, H. Y., Komossa, S., et al. 2008, *ApJ*, 685, 801. doi:10.1086/591046
- Zechmeister, M., & Kürster, M. 2009, *A&A*, 496, 577
- Zhang, B.-K., Zhao, X.-Y., Wang, C.-X., Dai, B.-Z., 2014, *Research in Astronomy and Astrophysics*, 14, 933
- Zhang, P.-F., Yan, D.-H., Liao, N.-H., Wang, J.-C., 2017a, *ApJ*, 835, 260
- Zhang, P.-F., Yan, D.-H., Liao, N.-H., Zeng, W., Wang, J.-C., Cio, L.-J., 2017b, *ApJ*, 842, 10
- Zhang, P.-F., Yan, D.-H., Zhou, J.-N., Fan, Y.-Z., Wang, J.-C., Zhang, L., 2017c, *ApJ*, 845, 82
- Zhang, P., Zhang, P. F., Yan, J. Z., et al. 2017d, *ApJ*, 849, 9
- Zhang, P. F., Zhang, P., Liao, N. H., et al., 2018, *ApJ*, 853, 193
- Zhang, P.-F., Yan, D.-H., Zhou, J.-N., Wang, J.-C., Zhang, L., 2020, *ApJ*, 891, 163
- Zhang, J., Zhang, H. M., Zhu, Y. K., Yi, T. F., Yao, S., Lu, R. J., Liang, E. W., 2017, *ApJ*, 849, 42
- Zhou, H., Wang, T., Yuan, W., et al. 2006, *ApJS*, 166, 128
- Zhou, X.-L., Zhang, S.-N., Wang, D.-X., & Zhu, L. 2010, *ApJ*, 710, 16
- Zhou, X.-L., Yuan, W., Pan, H.-W., & Liu, Z. 2015, *ApJL*, 798, L5
- Zhou, J. N., Wang, Z. X., Chen, L., et al. 2018, *NatCo*, 9, 4599